A Broadband Dual Circularly Polarized Conical Four-arm Sinuous Antenna

Shufeng Zheng, Member, IEEE, Steven Gao, Senior Member, IEEE, Yingzeng Yin, Qi Luo, Member, IEEE, Xiaodong Yang, Member, IEEE, Wei Hu, Member, IEEE, and Fan Qin

Abstract—A novel wideband four-arm sinuous antenna with dual circular polarizations and unidirectional radiation is proposed. Different from the conventional designs, this presented sinuous antenna is realized in a conical form and no absorptive cavity is needed to obtain unidirectional radiation. The beamforming network for dual circularly polarized operations consists of a wideband quadrature coupler and two wideband baluns, which are integrated within the sinuous aperture. The design of baluns and coupler is inspired from the printed exponentially tapered microstrip balun and broadside coupled microstrip coupler, respectively. Dynamic differential evolution (DDE) algorithm is employed to optimize the geometry of coupler for optimal performance. In both polarizations, the presented antenna has wide impedance bandwidth of 2-5GHz, good axial ratio (AR), moderate realized gain, and front-to-back ratio (FBR). An antenna prototype is fabricated and tested. The agreement between simulation and measurement results validates the proposed antenna framework. The demonstrated antenna is of light-weight, low-cost, and can be used in applications where wideband operation with dual circular polarizations and unidirectional radiation are required.

Index Terms—Conical, dynamic differential evolution (DDE), dual circular polarization, frequency independent (FI) antenna, sinuous antenna, wideband coupler.

I. INTRODUCTION

Broadband antennas capable of radiating waves with two orthogonal senses of polarizations are highly desirable in some applications such as electronic warfare, radio astronomy, and remote sensing systems [1]. Frequency independent (FI) antennas are potential solutions due to their invariant impedance and radiation characteristics over several octaves [1]-[3]. Spiral antennas [4]-[7] and log-periodic (LP) antennas [8]-[11] are the most commonly used two types of FI antennas. However, conventional spiral antennas can only radiate left-handed circular polarization (LHCP) or right-handed circular polarization (RHCP) waves with the sense of polarization specified by the winding direction of spirals. Although two-arm LP antennas are inherently linearly polarized, and FI dual polarized mode can be achieved by constructing a multi-arm structure with proper excitations, LP antennas are usually large, which constrains their applications. Some methods were proposed to address this problem. The modulated arm width (MAW) spiral antenna was designed to have dual CP operation of FI modes [7]. A miniaturized LP antenna loaded with a coupling ring was proposed in [11], although the true FI principles are not maintained before the turn-on frequency determined by the original LP structure. Sinuous antennas, which evolve from log-spiral antennas and LP antennas, are another type of FI antennas [12]. Owing to the interleaved structure, sinuous antennas have much smaller aperture sizes compared with LP antennas.

Most studies on sinuous antennas were devoted to the planar framework [13]-[18], for which supporting structures need to be designed to obtain unidirectional radiation. For example, a reflective cavity is backed behind the slot sinuous antenna, with the impedance bandwidth deteriorated [14]. Absorptive cavities can be used for less degraded bandwidth, but the addition of absorber inevitably causes severe reduction of gain, since the planar sinuous apertures are bidirectional [15]-[16]. Sinuous aperture can be printed on a dielectric lens to redirect the majority of radiated power to one side, but the loaded lens is bulky and inconvenient to fabricate [17]-[18]. It was pointed out in [12] that conical sinuous structure can radiate unidirectionally with its frequency independence retained. A conical two-arm sinuous antenna was presented in [19], but it was not frequency independent and alternating polarization handedness between adjacent bands was obtained. In [20], a conical four-arm sinuous aperture printed on an inverted cone with ground plane backed was proposed to achieve wideband operation, although the presence of ground plane destroyed the frequency independence of impedance.

In this paper, a novel conical four-arm sinuous antenna that unidirectionally radiates LHCP and RHCP waves at frequencies 2-5GHz is proposed. This work is an extension of the study presented in [21], where the design concept of the conical four-arm sinuous antenna was reported with some preliminary simulation results. In this work, deeper theoretic analysis and feasible beamforming network that excites sinuous arms for dual circularly polarized operations are presented. The beamforming network is composed of two printed exponentially tapered microstrip baluns and a broadside coupled microstrip quadrature coupler. Dynamic differential evolution (DDE) is employed to optimize the geometry of coupler for minimum deviation of two quadrature outputs over the desired frequency range. This developed antenna is characterized theoretically and experimentally, exhibiting the advantages of wide impedance bandwidth, good AR, moderate realized gain and FBR for both senses of circular polarizations. To the best knowledge of the authors, this is the first implementation of a conical four-arm sinuous antenna operated in the FI modes. This paper is organized as follows: the principles of operation of the sinuous antenna including the radiating ring theory, eigen-mode excitations and beamforming

network are presented in section II. The modeling and simulation of sinuous aperture and beamforming network are discussed in section III. In section IV, measurement and discussion are presented. A concluding remark is given in the last section.

II. THEORY OF OPERATION

A. Sinuous aperture

The proposed conical sinuous antenna is designed based on the spatial quasi-log sinuous curve, which is the projection of a planar quasi-log sinuous curve [12] on a cone, given by

$$\begin{cases} \varphi(r) = (-1)^p \alpha_p \sin\left[\dfrac{\pi \ln(\dfrac{r}{R_p})}{\ln(\tau_p)}\right], R_{p+1} \le r \le R_p \\ z(r) = H\dfrac{r - R_K}{R_K - R_1} \end{cases} \quad (1)$$

where r, φ and z are the cylindrical coordinates of the curve, and H is the height of cone; p is the number of segment and varies between 1 and K-1; α_p represents the angular width of each segment. τ_p represents the growth rate of each segment and can be set to vary in a linear way so that the arms are wound more closely at the outer edge of the aperture, given as

$$\tau_p = R_{p+1}/R_p = \tau_1 - \Delta\tau \cdot (p-1) \quad (2)$$

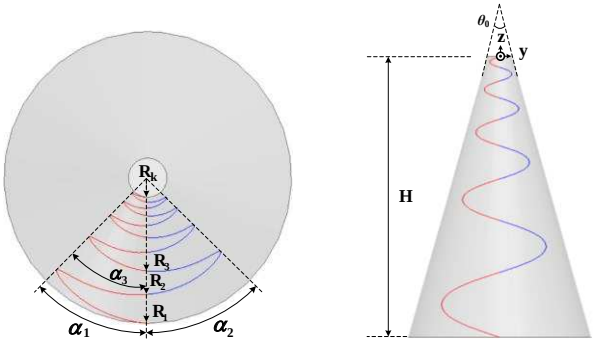

(a) Top view (b) Front view

Fig.1 Spatial quasi-log sinuous curve

The spatial sinuous curve, as shown in Fig.1, is rotated by $\pm\delta$ with respect to the axis of the cone to form one arm, which is then duplicated rotationally with 2π/N increments to construct N-arm sinuous aperture. Fig.2 shows the top view of the conical four-arm sinuous aperture.

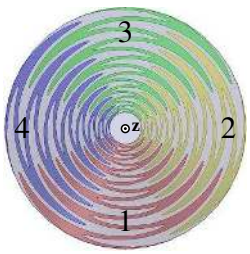

Fig.2 Top view of conical four-arm sinuous aperture

Similar to spiral antennas, principles of operation of tight interleaved circularly polarized sinuous aperture can be explained by using the radiating ring theory and eigen-mode excitations [1]. For an N-arm sinuous aperture fed at its center, outward travelling wave currents propagate along zigzag arms and dominant radiation occurs at the first active region where the circumference of the fictitious radiating ring approximates $m\lambda$, where m is the number of the desired mode and λ is the guided wavelength of the travelling wave. Residual currents are expected to attenuate remarkably before reaching the next active region or the ends of sinuous arms. In fact, besides the first active region, the travelling wave currents will also radiate efficiently, if the size of sinuous aperture permits, at other active regions with the circumferences approximating $(m+kN)\lambda$, where k is a positive integer. It is usually necessary to eliminate the radiation from the high-order radiating ring since they will distort the desired radiation pattern and decrease the gain. On the other hand, if the sinuous aperture is not large enough, residual currents will be reflected at the ends and propagate backwards, which will increase the cross-polarization radiation and may affect the impedance matching.

According to the radiating ring theory, a sinuous aperture should be truncated at the proper position, to support the first active region, avoid the excitation of high-order active regions and diminish the end effect. The radii of active regions enlarge as the operating frequency decreases. As a result, the highest and lowest operating frequencies of the sinuous aperture are virtually determined by the radius of top and bottom circle of the cone. Suggested values are given as [12]

$$\begin{cases} R_1 = \dfrac{\lambda_L}{4(\alpha_1 + \delta)} \\ R_K = \dfrac{\lambda_H}{8(\alpha_K + \delta)} \end{cases} \quad (3)$$

where λ_L and λ_H are the guided wavelength for the lowest and highest operating frequency. In practice, these values should be altered to diminish the truncation effect at the ends and feed points of the sinuous aperture. It is claimed that in [1], for higher efficiency, the radius of spiral antenna corresponding to lower frequency limit should be increased to

$$R_1 = \frac{(m_H + 1)\lambda_L}{2\pi} \quad (4)$$

where m_H is the mode order of the highest desired mode of operation. This rule also holds for tightly interleaved sinuous aperture.

The conical spiral antenna was firstly proposed in [5] to suppress the backwards radiation and increase the radiation toward cone apex. Likewise, directivity and the front-to-back ratio (FBR) of the conical sinuous antenna is also increased as the flare angle of the cone (θ_0) is reduced.

Different modes of operation can be realized with eigen-mode excitations (or characteristic feedings) to sinuous arms. Since an arbitrary excitation can be regarded as a combination of eigen-mode excitations, it is convenient to analyze the mode of operation with eigen-mode excitation. For an N-arm sinuous

aperture with rotational symmetry, provided the number of the desired mode is m, the desired excitation is given as [22]

$$I_{k,m} = I_{0m} e^{\frac{-j2\pi m(k-1)}{N}} \quad (5)$$

where k = 1, … , N denotes the arm number, and I_{0m} is a constant amplitude of the current. The current conservation condition should be satisfied, given by

$$\sum_{k=1}^{N} I_{k,m} = 0 \quad (6)$$

From equation (5) and (6), it can be concluded that only N-1 feasible eigen-mode excitations can be realized for the N-arm sinuous antenna. Specifically, for the 4-arm cone sinuous aperture shown in Fig.2, the required excitation for mode 1 is $I_{01}\{1, j, -1, -j\}$, which produce the LHCP radiation toward +z direction. The excitation of $I_{03}\{1, -j, -1, j\}$ is needed for mode 3 (or mode -1) which corresponds to the RHCP radiation toward +z direction. It is interesting to point out that according to the excitation of mode 2 (also called differential mode since a radiation null emerges in the broadside direction), i.e. $I_{02}\{1, -1, 1, -1\}$, the sense of polarization of this 4-arm sinuous aperture is indistinguishable. In fact, to support M FI modes without ambiguity of polarization, at least 2M+1 arms are required for a sinuous aperture. Therefore, at least 3 arms are needed for dual CP applications, and 4-arm structures are the most commonly used considering the complexity of beamforming network.

B. Beamforming network

To achieve dual CP for the conical 4-arm sinuous aperture shown in Fig.2, required excitations for mode +1 and mode -1 have to be realized simultaneously. A beamforming network illustrated in Fig.3 (a) can be utilized to provide the desired excitations. Due to the quadrature characteristics (equal in magnitude and orthogonal in the phase of the two outputs when the signal is input at LHCP or RHCP port) of coupler and phase inversion characteristics of baluns, desired excitations to each arm for both polarizations can be accomplished. Baluns also provide the necessary impedance transformation of sinuous arms from their input impedances seen from the feed points of the sinuous aperture into port impedances of the coupler. The input impedance of sinuous antenna for different modes can be determined by using Deschamps' formula [23]. For a self-complementary N-arm structure in free space, the input impedance of a single arm to the ground is

$$Z_m = \frac{\eta_0}{4\sin(\frac{m\pi}{N})} \quad (7)$$

where $\eta_0 = 120\pi\ \Omega$ is the intrinsic impedance of free space and m is the mode of operation. According to equation (7), impedances across arm 1 and arm 3 (also arm 2 and arm 4) for mode +1 and mode -1 are computed to be 266Ω. Note that the dielectric loading of supporting substrate can decrease the theoretical values.

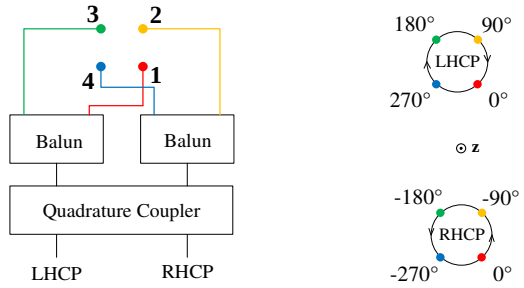

(a) Framework of beamforming network (b) Resulting excitations

Fig.3 Framework of beamforming network and resulting excitations for dual circular polarization operation

III. Simulations and Performance Analysis

As shown in Fig.4, the proposed conical sinuous antenna consists of sinuous aperture (with feeding patch), baluns and coupler. The simulated results of these modules and their integrations are presented in this section.

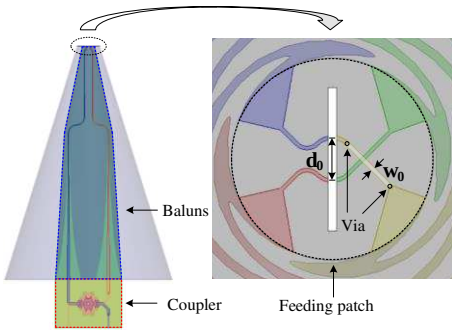

Fig.4 Antenna geometry (sinuous arms are not shown for clarity) and zoomed-in view of feeding patch

A. Sinuous aperture

Since sinuous arms are constructed on a cone and it is difficult to connect them with the beamforming network directly, an auxiliary circular feeding patch is designed and positioned at the top of the cone. The stripes printed on the feeding patch are composed of straight and curved segments. One segment is etched on the opposite side of the patch and two vias are used to avoid the intersection. A narrow area of the feeding patch is removed to form a slot so that the baluns can be combined.

The outer and inner radius of sinuous aperture (i.e. R_1 and R_K) can be estimated by using formula (3) and (4). Note that these approximate values may vary for conical configuration. The height of the cone H is determined to obtain an FBR greater than 10dB. α_p is kept constant for each segment and δ is set to be π/N to maintain the self-complementarity. Structure parameters of the conical sinuous aperture are listed in Table I.

TABLE I. Geometry Parameters of the Sinuous Aperture.

Parameter	K	δ	α	τ_1	$\Delta\tau$
Value	16	22.5 deg	45 deg	0.9	0.005
Parameter	R_1	R_{16}	H	w_0	d_0
Value	50mm	5.7mm	150mm	0.2mm	3mm

Since the operation mechanism and design guidelines of sinuous aperture have been presented in section II, the parameter analysis is not given here for brevity. However, it is worthy to point out that the width of strips feeding four arms (w_0) is critical to the performance of sinuous aperture. As shown in Fig.5 and Fig.6, an increase of w_0 helps to decrease the input impedance but boresight AR becomes worse. In fact, due to the coupling of strips which feed four sinuous arms, the purity of polarization is contaminated and AR deteriorated consequently when w_0 is increased. Note that the analysis is based on LHCP case and results for RHCP case are similar. Therefore, they are not shown here for clarity.

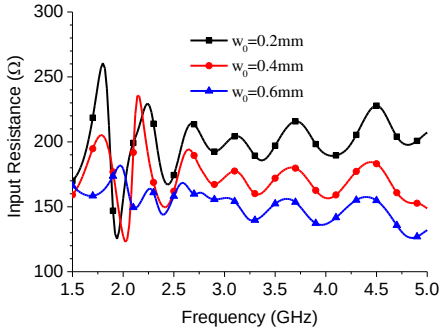

Fig.5 Simulated input resistance of sinuous aperture with the various values of w_0 (LHCP case)

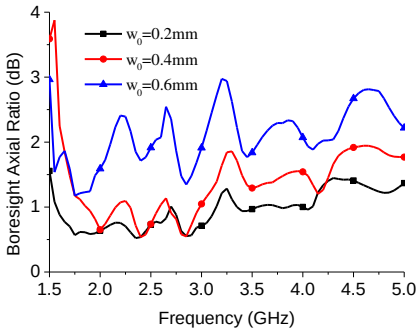

Fig.6 Simulated boresight axial ratio of sinuous aperture with the various values of w_0 (LHCP case)

B. Beamforming Network

As indicated in Fig.3, printed parallel stripe line is an attractive candidate to feed the sinuous arms from the viewpoint of symmetry of excitations. On the other hand, wideband quadrature coupling characteristics of the coupler are critical to realize dual CP operations. Therefore, broadside coupled microstrip line coupler and printed exponentially tapered microstrip baluns are proposed to constitute the beamforming network, considering their inherent wideband property and ease of connection.

The geometry of baluns is shown in Fig.7 and relevant parameters are listed in Table II. Note that necessary modifications of the structure are applied to facilitate the assembly with the conical sinuous aperture.

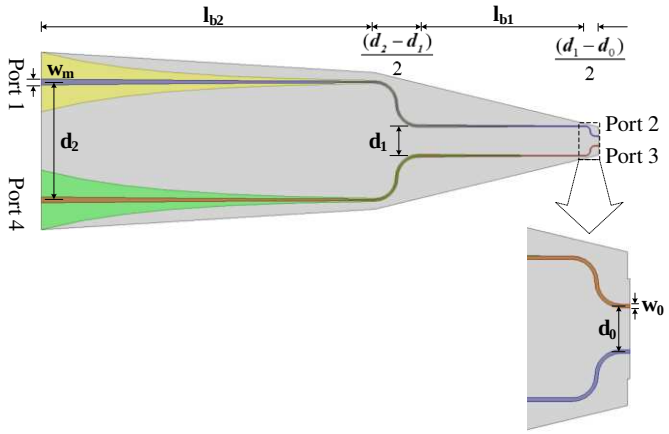

Fig.7 Geometry of modified exponentially tapered microstrip balun

TABLE II. GEOMETRY PARAMETERS OF THE BALUN.

Parameter	d_1	d_2	l_{b1}	l_{b2}	w_m
Value (mm)	10	31.76	90	45	1.6

Simulated results of the designed baluns are given in Fig.8, from which it can be seen that insertion loss is less than 1dB, reflection coefficient less than -17dB, and isolation better than 24dB at frequencies 2-5GHz.

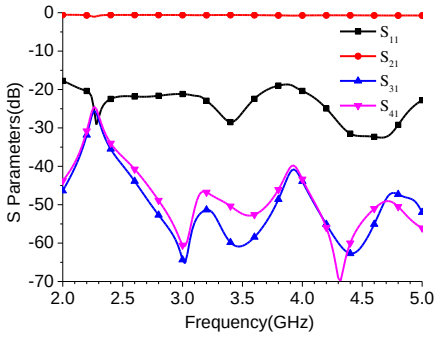

Fig.8 Simulated S parameters of exponentially tapered microstrip balun

Wideband quadrature coupling characteristics of the proposed coupler are realized by broadside coupled microstrip lines. As shown in Fig.9, two patterned microstrip lines are coupled through the patterned aperture on their common ground plane. When current is input at port 1, output currents at port 2 and port 3 have equal magnitude and orthogonal phases, while port 4 is the isolated port. Two vias are used to transfer the microstrip traces to the opposite layer so that it can be directed to the baluns directly. Consequently, compensation sections (bent microstrip trace sections) are needed to correct the phase deviation caused by the vias. The hole at the center of the coupler is reserved for the ease of assembly.

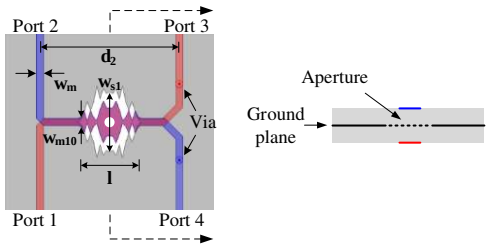

Fig.9 Geometry of broadside coupled microstrip coupler

In this paper, the patterned microstrip lines and aperture are composed of fragmented sections, and DE algorithm [24] is employed to optimize their sizes. It was demonstrated in [25] that the control parameters are critical to the performance of DE and it is beneficial to change them dynamically or adaptively during the evolution process. A simple yet efficient DE is used here, of which the mutation scale factor (F) and crossover factor (CR) change dynamically against the generation while the population size (NP) is kept fixed during the evolution process. More specifically, F decreases while CR increases in a non-linear way so as to balance the exploration and exploitation ability of the algorithm at different stages of optimization process, given by

$$\begin{cases} F = F_0 \cdot 2^{\lambda} \\ \lambda = e^{-\frac{G}{G_{max}+1-G}} \end{cases} \tag{8}$$

$$\begin{cases} CR = CR_{min} + (CR_{max} - CR_{min}) \cdot e^{\alpha} \\ \alpha = -a\left(1 - \frac{G}{G_{max}}\right)^{b} \end{cases} \tag{9}$$

where F_0, CR_{min} and CR_{max} are pre-defined parameters to set F and CR. G is the number of generation and G_{max} the maximum generation. a and b are pre-defined constants. The control parameters of this proposed DDE are listed in Table III.

TABLE III. CONTROL PARAMETERS OF DDE.

Parameter	NP	F_0	CR_{min}	CR_{max}	G_{max}	a	b
Value	105	0.9	0.3	0.9	500	30	3

The objective of this optimization is to minimize the imbalance of two quadrature outputs, reflection at input port, and coupling at isolated port, so the fitness function can be defined as

$$\begin{cases} F(\vec{x}) = c_1 \cdot \max\limits_{f \in [f_{min}, f_{max}]} \{ |S_{21}(\vec{x}) - ref| + |S_{31}(\vec{x}) - ref| \} \\ \qquad + \dfrac{c_2}{|\max\limits_{f \in [f_{min}, f_{max}]} \{S_{11}(\vec{x})\}|} + \dfrac{c_3}{|\max\limits_{f \in [f_{min}, f_{max}]} \{S_{41}(\vec{x})\}|} \\ \vec{x} = (l, w_{s1} \sim w_{s10}, w_{m1} \sim w_{m10}) \end{cases} \tag{10}$$

The coupled microstrip lines and coupling aperture are fragmented into 20 sections with the same length, and kept symmetrical on their centerlines, so $\vec{x}$ is a 21-dimensional vector representing design solutions. ref is the reference value and set to be -3.2dB considering the loss and reflection. c_1, c_2 and c_3 are the weights of magnitude imbalance of two quadrature outputs, return loss and isolation, and set to be 1. The optimized geometry parameters of coupler and corresponding scattering parameters are presented in Table IV and Fig.10, respectively. Fig. 10 shows that the magnitude of S_{21} change between -3.8dB and -2.7dB, while the magnitude of S_{31} change between -3.6dB and -2.8dB, and the difference of magnitude is less than 1dB at frequencies 2-5GHz. On the other hand, the phase difference varies between 88 degrees and 93 degrees at these frequencies. The reflection coefficient and isolation is better than -18dB and -17dB respectively at these frequencies. Therefore, favorable quadrature coupling characteristic is obtained over the desired frequency range.

TABLE IV. THE GEOMETRY OF COUPLER.

Parameter	l	w_{s1}	w_{s2}	w_{s3}	w_{s4}	w_{s5}	w_{s6}
Value (mm)	14.56	6.78	6.39	7.57	5.2	8.09	4.56
Parameter	w_{s7}	w_{s8}	w_{s9}	w_{s10}	w_{m1}	w_{m2}	w_{m3}
Value (mm)	2.6	4.59	2.22	0.43	3.15	3.25	4.77
Parameter	w_{m4}	w_{m5}	w_{m6}	w_{m7}	w_{m8}	w_{m9}	w_{m10}
Value (mm)	2.88	0.34	1.02	2.57	0.21	2.47	1.07

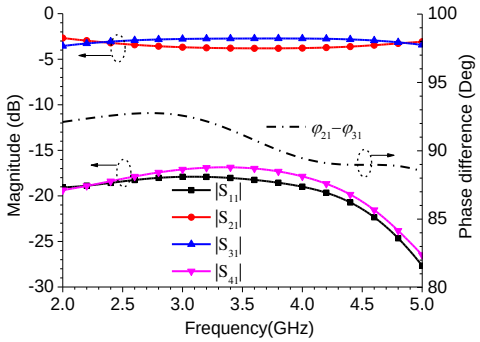

Fig.10 Simulated S parameters of broadside coupled microstrip coupler

C. Sinuous Antenna with Beamforming Network

After designing sinuous aperture and its beamforming network, it is necessary to combine them together and analyze the performance as a whole. By geometrical refinements of aperture, baluns and coupler to ensure interconnectivity between these modules, it is a quite straightforward way to construct the sinuous antenna with beamforming network, as shown in Fig.4.

The simulated values of active VSWR and boresight axial ratio of LHCP and RHCP operations are less than 2 and 3dB, respectively, at frequencies 2-5GHz, as shown in Fig.11 and Fig.12. The simulated co-pol and cross-pol realized gain in boresight direction for LHCP and RHCP excitations are presented in Fig.13. It shows that the realized co-pol gains for both polarizations are between 6-8.2dB, and their corresponding co-pol gain is at least 15dB lower over the frequencies 2-5GHz. Simulated radiation patterns of the sinuous antenna for LHCP and RHCP excitations are shown in Fig.14 and Fig.15, respectively. It can be observed that radiation patterns are quite stable over the frequency range, and FBR is better than 10dB for the presented frequencies. The simulated results indicate that the designed sinuous antenna

exhibits good dual circular polarizations feature at the desired frequencies, and performance of LHCP and RHCP operations are quite similar.

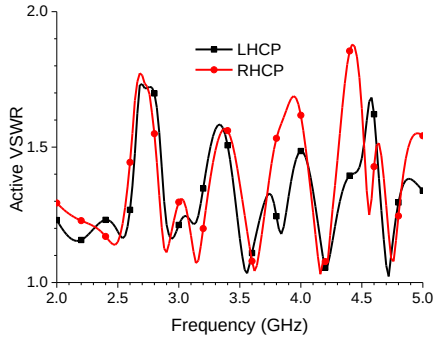

Fig.11 Simulated active VSWR of sinuous antenna

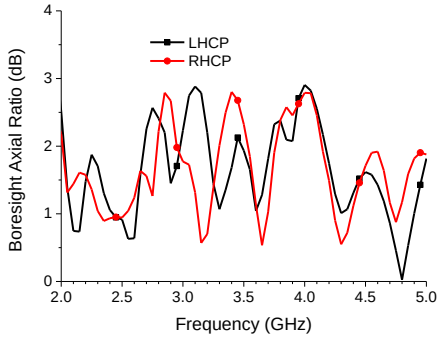

Fig.12 Simulated boresight axial ratio of sinuous antenna

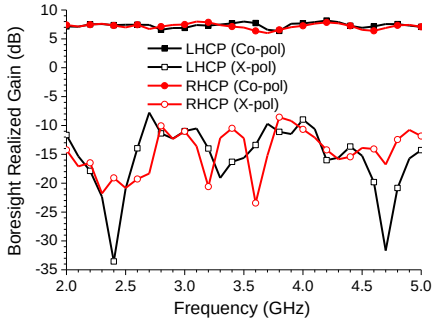

Fig.13 Simulated boresight realized gain of sinuous antenna

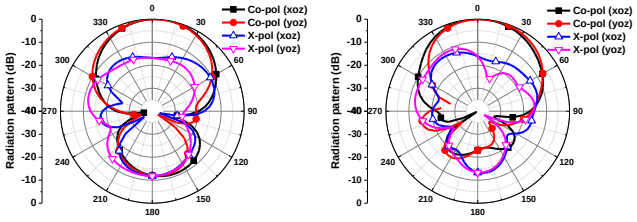

(a) (b)

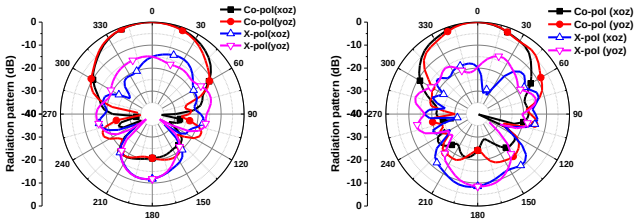

(c) (d)

Fig.14 Simulated radiation pattern of sinuous antenna with LHCP excitation at (a) 2GHz; (b) 3GHz; (c) 4GHz; (d) 5GHz.

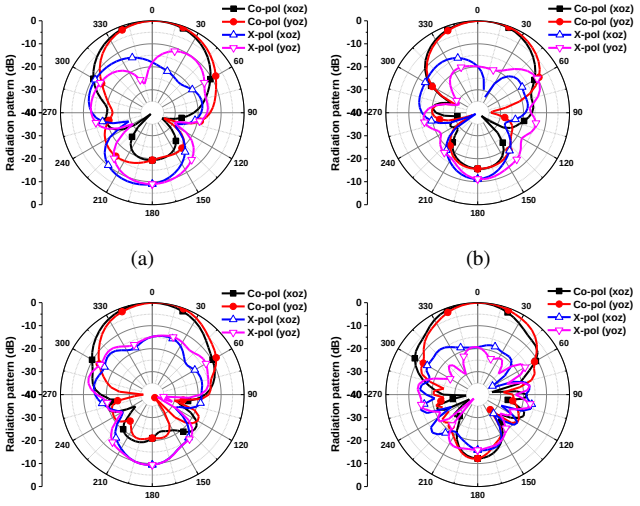

(a) (b)

(c) (d)

Fig.15 Simulated radiation pattern of sinuous antenna with RHCP excitation at (a) 2GHz; (b) 3GHz; (c) 4GHz; (d) 5GHz.

IV. MEASUREMENTS AND DISCUSSION

Considering the performance of wideband quadrature coupler is critical to the outcome of the dual polarized sinuous antenna, a prototype of the optimized quadrature coupler is fabricated and tested before the fabrication of sinuous antenna with beamforming network, as presented in Fig.16. The prototype is printed on an Arlon Cuclad217 substrates (ε_r=2.17, and tanδ=0.0009) with a thickness of 0.508mm. The measured S-parameters shown in Fig.17 agree well with the simulated results. It can be observed that difference of magnitude is less than 1.1dB, and the phase difference is between 85 degrees and 95.5 degrees at frequencies 2-5GHz. Return loss and isolation are better that 14.5dB.

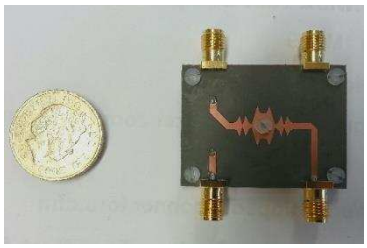

Fig.16 Photo of quadrature coupler prototype

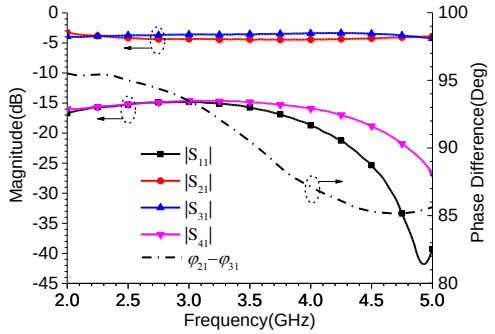

Fig.17 Measured S-parameters of quadrature coupler prototype

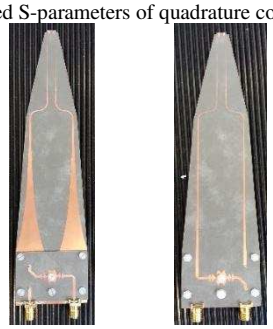

(a) (b)

Fig.18 Photo of fabricated beamforming network composed of baluns and quadrature coupler (a)Front view; (b)Back view.

As aforementioned, the quadrature coupler and two baluns constitute the beamforming network, so the baluns are printed on one of two dielectric substrates consisting of the coupler, as shown in Fig.18. To excite conical four sinuous arms, the beamforming network is inserted into the narrow slot cut on the feeding patch and positioned perpendicularly underneath the cone. Four sinuous arms are printed on a Kapton substrate (ε_r=3.8, and tanδ=0.0036) with a thickness of 0.125mm and wrapped into a cone. Foam layers are used as fixtures besides solderings on feeding patch. Shown in Fig.19 is the sinuous antenna prototype under test for active VSWR and far-field performance.

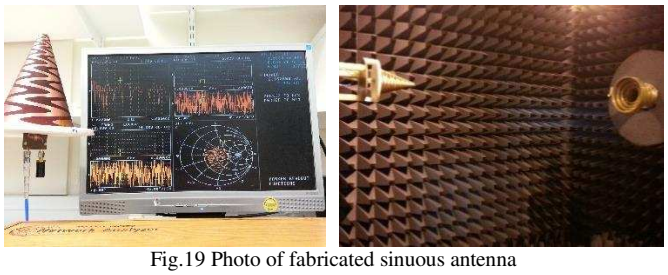

Fig.19 Photo of fabricated sinuous antenna

The measured active VSWR of the sinuous antenna prototype is plotted in Fig.20, which shows that the active VSWR are smaller than 2.3 at frequencies 2-5GHz for LHCP and RHCP excitations. Presented in Fig.21 are measured AR and co-pol gain in boresight direction for each case of port excitation. It can be observed that boresight AR are less than 4dB and boresight co-pol gain vary between 5.3dB and 7.5dB at frequencies 2-5GHz for both cases. Measured radiation patterns of the sinuous antenna for LHCP and RHCP excitations are shown in Fig.22 and Fig.23, respectively. Stable patterns are obtained for both cases of polarizations within the frequency range and acceptable consistency between two cases are achieved. The difference between two cases is mainly caused by the asymmetry of the structure of feeding patch and coupler, fabrication tolerance and inaccuracy of assembly.

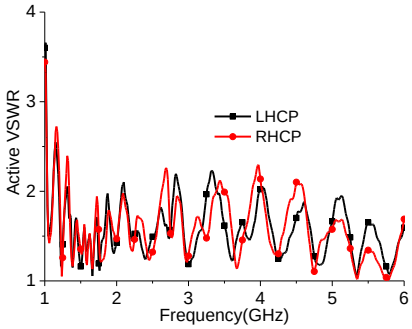

Fig.20 Measured active VSWR of sinuous antenna prototype

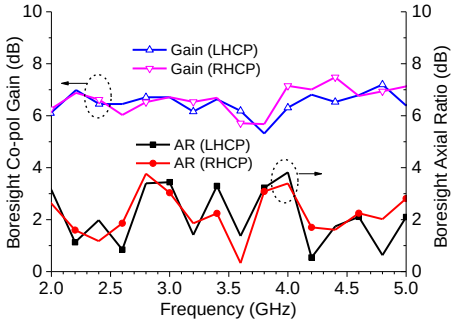

Fig.21 Measured boresight axial ratio and gain of sinuous antenna prototype

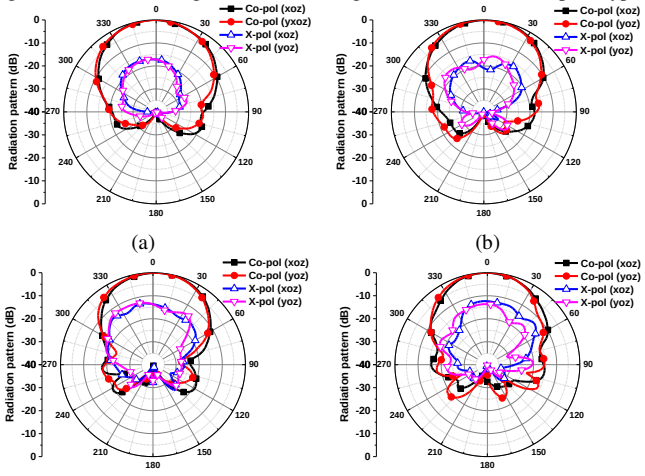

(a) (b) (c) (d)

Fig.22 Measured radiation pattern of sinuous antenna with LHCP excitation at (a) 2GHz; (b) 3GHz; (c) 4GHz;(d) 5GHz.

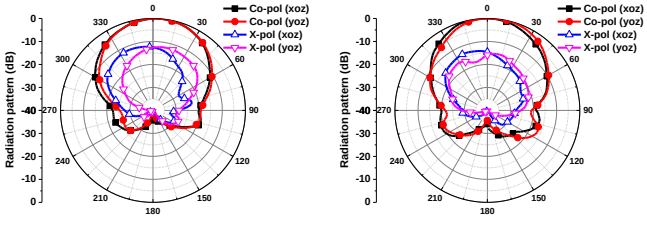

(a) (b)

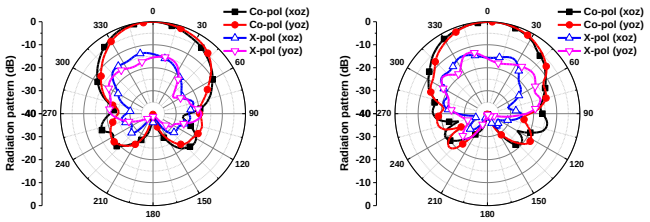

(c) (d)

Fig.23 Measured radiation pattern of sinuous antenna with RHCP excitation at (a) 2GHz; (b) 3GHz; (c) 4GHz; (d) 5GHz.

Simulation analysis indicates that the bandwidth of the proposed sinuous antenna is mainly limited by that of quadrature coupler. Nevertheless, the obtained results demonstrate the validity of the proposed framework that conical four-arm sinuous antenna can unidirectionally radiate LHCP and RHCP waves efficiently without the necessity of absorptive cavity or loaded lens, which provide a potential solution for applications where light-weighted low-cost broadband dual circularly polarized antennas are demanded.

V. CONCLUSION

A conical four-arm sinuous antenna is proposed in this paper. The sinuous aperture is constructed on a cone for unidirectional radiation, and a beamforming network for dual circular polarizations operations is also presented. The beamforming network consists of two printed exponentially tapered microstrip baluns and a broadside coupled microstrip quadrature coupler. Dynamic differential evolution algorithm is utilized to optimize the geometry of coupler for minimum deviation of two quadrature outputs over the desired frequency range. An auxiliary feeding patch is designed to facilitate the connection between sinuous arms and baluns. The performance of sinuous aperture and beamforming network is simulated respectively, and their combination is also analyzed. Prototypes of the coupler and sinuous antenna were fabricated and measured. Good agreement between measurement and simulation results are achieved, indicating that the proposed conical four-arm sinuous antenna provide an efficient solution for unidirectional radiation of wideband dual circularly polarized signals without the necessity of absorptive cavity.

ACKNOWLEDGEMENT

This work was partly supported by the National Natural Science Foundation of China (No. 61501340). The authors would like to thank Mr Simon Jakes and Mr Antonio Mendoza at the University of Kent for their help in antenna prototyping and measurements.

REFERENCES

[1] Oliner, Arthur A., David R. Jackson, and J. L. Volakis. "Antenna Engineering Handbook." McGraw Hill (2007).

[2] Rumsey, V., "Frequency Independent Antennas," IRE International Convention Record. 1957, Vol. 5, pp. 114–118.

[3] Mayes, Paul E. "Frequency-independent antennas and broad-band derivatives thereof." Proceedings of the IEEE 80.1 (1992): 103-112.

[4] Dyson, J., "The equiangular spiral antenna," Antennas and Propagation, IRE Transactions on , vol.7, no.2, pp.181-187, April 1959.

[5] Dyson, John D. "The unidirectional equiangular spiral antenna." Antennas and Propagation, IRE Transactions on 7.4 (1959): 329-334.

[6] Kaiser, Julius. "The Archimedean two-wire spiral antenna." Antennas and Propagation, IRE Transactions on 8.3 (1960): 312-323.

[7] P. G. Ingerson, ″Modulated arm width spiral antenna,″ U. S. Patent 3,681,772, Aug. 1, 1972.

[8] DuHamel, Raymond, and Dwight Isbell. "Broadband logarithmically periodic antenna structures." 1958 IRE International Convention Record. Vol. 5. IEEE, 1966.

[9] Isbell, Dwight E. "Log periodic dipole arrays." Antennas and Propagation, IRE Transactions on 8.3 (1960): 260-267.

[10] Cortes-Medellin, German. "Non-planar quasi-self-complementary ultra-wideband feed antenna." Antennas and Propagation, IEEE Transactions on 59.6 (2011): 1935-1944.

[11] Sammeta, Rohit, and Dejan S. Filipovic. "Quasi frequency-independent increased bandwidth planar log-periodic antenna." Antennas and Propagation, IEEE Transactions on 62.4 (2014): 1937-1944.

[12] DuHamel R. H., Dual Polarized Sinuous Antennas, U.S. Patent 4658 262, Apr. 14, 1987.

[13] Waldschmidt, Christian, and Werner Wiesbeck. "Compact wide-band multimode antennas for MIMO and diversity." Antennas and Propagation, IEEE Transactions on 52.8 (2004): 1963-1969.

[14] Buck, Michael C., and Dejan S. Filipović. "Split-beam mode four-arm slot sinuous antenna." Antennas and Wireless Propagation Letters, IEEE 3.1 (2004): 83-86.

[15] S. Palreddy, A. I. Zaghloul, and R. Cheung, “An optimized lossy back cavity loaded four arm sinuous antenna,” in Proc. IEEE Antennas Propag. Symp., Toronto, ON, Canada, Jul. 2010.

[16] Sammeta, Rohit, and Dejan S. Filipovic. "A low-profile sinuous antenna." Antennas and Propagation Society International Symposium (APSURSI), 2014 IEEE. IEEE, 2014.

[17] Edwards, Jennifer M., et al. "Dual-polarized sinuous antennas on extended hemispherical silicon lenses." Antennas and Propagation, IEEE Transactions on 60.9 (2012): 4082-4091.

[18] Sammeta, Rohit, and Dejan S. Filipovic. "Improved Efficiency Lens-Loaded Cavity-Backed Transmit Sinuous Antenna." Antennas and Propagation, IEEE Transactions on 62.12 (2014): 6000-6009.

[19] Buck, Michael C., and Dejan S. Filipović. "Two-arm sinuous antennas." Antennas and Propagation, IEEE Transactions on 56.5 (2008): 1229-1235.

[20] R. Gawande and R. Bradley, “Towards an ultra-wideband low noise active sinuous feed for next generation radio telescopes,” IEEE Trans. Antennas Propag., vol. 59, no. 6, pt. 1, pp. 1945–1953, Jun. 2011.

[21] S. Zheng, Z. Wang, X. Ren and S. Gao, "A conical four-arm sinuous antenna," 2015 IEEE International Symposium on Antennas and Propagation & USNC/URSI National Radio Science Meeting, Vancouver, BC, 2015, pp. 1986-1987.Sussman, Raphael Sivan. "Various modes of the equiangular spiral antenna." Antennas and Propagation, IEEE Transactions on 11.5 (1963): 533-539.

[22] Deschampes, G., "Impedance Properties of Complementary Multiterminal Planar Structures," IEEE Transactions on Antennas and Propagation. 1959, Vol. 7, 5.

[23] P. Rocca, G. Oliveri and A. Massa, "Differential Evolution as Applied to Electromagnetics," in IEEE Antennas and Propagation Magazine, vol. 53, no. 1, pp. 38-49, Feb. 2011

[24] U. K. Chakraborty, Advances Differential Evolution, Heidelberg, Germany: Springer-Verlag, 2008.